A Pharmacokinetic Modeling Approach to Predict the Contribution of Active Metabolites to Human Efficacious Dose

Authors:

Iain J. Martin, Susan E. Hill, James A. Baker, Sujal V. Deshmukh and Erin F. Mulrooney

Affiliations:

Pharmacokinetics, Pharmacodynamics, and Drug Metabolism, Merck Research Laboratories,

Boston, MA, 02115. Current affiliation: Metabolism and Pharmacokinetics, Novartis Institutes for

Biomedical Research, Cambridge, MA 02139 (S.E.H., S.V.D.)

Running Title: PK modeling of active metabolites

Corresponding author:

Iain J. Martin

Merck Research Laboratories, 33 Avenue Louis Pasteur, Boston, MA 02115, USA

e-mail: iain.martin@merck.com

phone: +1-617-992-2509

fax: +1-617-992-2485

23 text pages

1 table

4 figures

35 references

Abstract- 247 words

Introduction- 438 words

Discussion- 1466 words

Abbreviations:

AUC, area under the plasma concentration time curve; CL, plasma clearance; fabs, oral fraction absorbed; ka, absorption rate constant; LC-MS/MS, liquid chromatography-mass spectrometry; MRK-1, Merck candidate drug parent compound; M1, active metabolite 1 of MRK-1; M2, active metabolite 2 of MRK-1; PK, Pharmacokinetics; Vss, volume of distribution at steady state

ABSTRACT

A preclinical drug candidate, MRK-1, was found to elicit tumor regression in a mouse xenograft model. Analysis of samples from these studies revealed significant levels of two circulating metabolites whose identities were confirmed by comparison to authentic standards using liquid chromatography-mass spectrometry (LC-MS/MS). These metabolites were found to have similar in vitro potency to MRK-1 against the pharmacological target and were therefore thought to contribute towards the observed efficacy. In order to predict this contribution in humans, a pharmacokinetic (PK) modeling approach was developed. At the efficacious dose, the mouse steady state unbound areas under the plasma concentration time curves (AUCs) of the active metabolites were normalized by their in vitro potency compared to MRK-1. These normalized metabolite AUCs were added to that of MRK-1 to yield a composite efficacious unbound AUC, expressed as 'parent drug equivalents', which was used as the target AUC for predictions of the human efficacious dose. In vitro and preclinical PK studies afforded predictions of the PK of MRK-1 and the two active metabolites in human as well as the relative pathway flux to each metabolite. These were used to construct a PK model (Berkeley Madonna, v 8.3.18, Berkeley Madonna Inc., University of California, Berkeley, CA) and predict the human dose required to achieve the target 'parent equivalents' exposure. These predictions were used to inform on the feasibility of the human dose in terms of size, frequency, formulation and likely safety margins as well as to aid design of preclinical safety studies.

3

INTRODUCTION

During drug discovery, predictions of human pharmacokinetics and efficacious dose are important for making decisions about a compound's probability of success in clinical development. Increasingly, such predictions are made as part of an integrated translational pharmacology strategy (Bueters *et al.*, 2015). Various methods for human PK predictions have been developed and refined, incorporating a range of in silico, in vitro and preclinical in vivo data and there are many excellent reviews on the subject (Obach *et al.*, 1997; Lombardo *et al.*, 2013a, 2013b). An understanding of metabolism and other clearance mechanisms in vitro and in preclinical species and how they translate to the clinic is a pivotal component of these predictions. Drug metabolites can not only cause or contribute to drug-drug interactions (Isoherranen, 2009;Yu and Tweedie, 2013; Yu *et al.*, 2015) and other safety concerns (Rambeck *et al.*, 1990; Ho *et al.,* 2003; Bauman *et al.*, 2008) but can also potentially contribute to efficacy (Drayer, 1976; Fura, 2006; Obach 2013). In such cases, predictions of human efficacious dose should include the contribution of active metabolites to efficacy.

In the current work, an oncology candidate compound (MRK-1) elicited tumor regression in a mouse xenograft model following repeated oral administration. It was apparent from in vitro and in vivo data that this compound, in common with most of the chemical series, underwent metabolism to produce significant levels of circulating metabolites. Since some of these metabolites (M1 and M2) were known to possess significant in vitro potency, it was important to assess their potential contribution to the observed efficacy in the mouse and how this might translate to the clinic. This would inform on projections of clinical efficacious dose as well as guide further optimization strategy. Here, an approach is described to quantifying the contribution of active metabolites to mouse efficacy and incorporating this into a model (built in Berkeley Madonna, version 8.3.18, Berkeley Madonna Inc., University of California, Berkeley, CA) to predict the human PK and efficacious dose. The objective of building this model was to provide a fit-for-purpose tool that the program team could use to predict the human efficacious dose and assess its feasibility in terms of size, frequency, formulation and likely safety margins.

Since the model output provided a predicted PK profile of both drug and the active metabolites, it

was also used to aid the design of preclinical safety studies. The model facilitated interrogation of

various "what if" scenarios and was applied to other molecules over the course of the drug

discovery program. The approach and model are generally applicable to active metabolite

scenarios and the full executable model code is made available (Supplemental Material 1).

MATERIALS AND METHODS

In this Materials and Methods Section, the focus will be on the approach used to predict and incorporate the contribution of active metabolites to the human efficacious dose together with a detailed description of the PK model. The full model code is available in the supplemental material (Supplemental Material 1) and can be executed in Berkeley-Madonna via a simple copy and paste. We will give only a brief overview of the methodology used to generate the model inputs since the precise details are not central to the applicability of the approach and the model. Other researchers can follow the approach and use the model by generating the appropriate model inputs using their own preferred methods.

Assumptions and Approach

It was assumed that efficacy was driven by free drug and that free drug concentrations in plasma were a surrogate for that in the tumor. Further, since in vitro potencies for the parent drug and active metabolites were within a 2.5-fold range, mutual competitive inhibition was not invoked. Rather, it was assumed that an efficacious response (tumor regression) could be equally driven by parent drug or an equivalent combined concentration of parent dug and active metabolites. The primary route of elimination for all three molecules was assumed to be via hepatic metabolism and the systemic availability of metabolites M1 and M2 was assumed to be 1.

The mouse steady state unbound plasma AUCs of the active metabolites at the efficacious dose were normalized by their in vitro potency relative to the parent compound. These normalized metabolite AUCs were added to that of the parent drug to yield a composite efficacious unbound AUC expressed in terms of 'parent drug equivalents'. This AUC was used as the target exposure for predictions of the human efficacious dose. In vitro and preclinical PK studies afforded predictions of the PK parameters of the parent compound and the two active metabolites in human as well as the relative metabolic pathway flux to each of the active metabolites. These predictions were combined with the relative in vitro potencies of parent compound and the active

6

metabolites in man to parameterize a PK model and estimate the human dose required to

achieve the target 'parent equivalents' exposure.

Model Structure

A system of differential equations was constructed in Berkeley Madonna (version 8.3.18,

Berkeley Madonna Inc., University of California, Berkeley, CA) to represent the flux through the

proposed metabolic pathways (Figure 1). A schematic of the model structure is presented in

Figure 2 and the full model code is available (Supplemental Material 1). An overview of the

generation of the model inputs is given below and these are summarized, together with their

numerical values, in Table 1. Readers can execute the model code by copying and pasting from

the supplemental material directly into a blank Berkeley Madonna equations page. Furthermore,

the approach and model are generally applicable and the reader may transpose them to their own

active metabolite scenario by consideration of Figure 2, creation of the appropriate model

structure, and subsequent editing of the model code.

Overview of generation of model input data.

All animal studies were performed using protocols approved by the Merck Institutional Animal

Care and Use Committee.

The putative metabolic pathway of MRK-1, M1 and M2 was elucidated by high resolution mass

spectrometry and LC-MS/MS analysis of incubates generated in microsomes and hepatocytes

(rat, dog, human) and recombinant human CYPs as well as of plasma from PK studies (rat, dog).

The primary in vitro potencies of MRK-1, M1 and M2 at the pharmacological target were

determined by immobilized metal ion affinity-based fluorescence polarization using the

phosphorylated active human enzyme. The in vivo efficacy of MRK-1 was assessed in a mouse

xenograft model in which human-derived tumor cells were implanted into the flank of female CD1

nude mice. Following a 3 week tumor establishing period, MRK-1 was administered as a

suspension by oral gavage at 25, 50 and 100 mg/kg b.i.d. for 21 days (n=5 per dose group). On

day 21, mice were sacrificed at 2, 4, 6, 9 and 24 h, blood samples collected and tumors excised.

Blood samples were centrifuged to yield plasma which was then analyzed by LC-MS/MS to

quantify MRK-1, M1 and M2. Tumors were measured using calipers and tumor volume was

calculated according to the algorithm: Volume = ½(Length x Width^2). The efficacious dose was

considered to be the minimum dose level that elicited tumor regression over the time course of

the study.

The in vitro intrinsic clearances of MRK-1, M1 and M2 were determined in cryopreserved rat, dog

and human hepatocytes using a standard substrate depletion method (eg: Naritomi *et al.,* 2003)

and quantified via LC-MS/MS. Compounds were incubated for 120 min at 0.3 µM in Krebs-

Henseleit buffer containing $2x10^6$ hepatocytes per mL and the initial slope of the substrate

disappearance curve (ln peak area ratio versus time) was used to calculate the intrinsic

clearance.   For MRK-1, M1 and M2, the contributions of the pathways yielding the active

metabolites (MRK-1→M1 & M2; M1→M2; M2→M1) were estimated by monitoring the metabolite

appearance in cryopreserved rat, dog and human hepatocytes at a substrate concentration of

1 µM. Metabolite concentrations were quantified by LC-MS/MS using a standard curve prepared

from authentic standards and the initial metabolite formation rate was calculated from the linear

portion of the appearance curve. This rate was divided by the substrate concentration to yield an

estimate of formation intrinsic clearance. The fractional contribution of each metabolite to the

total elimination was determined by dividing its formation intrinsic clearance by the depletion

intrinsic clearance of its parent molecule. Any substrate depletion intrinsic clearance not

accounted for by formation of the monitored metabolites was assigned to pathways resulting in

inactive metabolites.

Plasma protein binding of MRK-1, M1 and M2 was determined in mouse, rat, dog and human

plasma by equilibrium dialysis using the HTDialysis apparatus (HTDialysis LLC, Gales Ferry, CT);

compounds were incubated for 6 h at a concentration of 1 µM. Blood to plasma ratios were

determined in fresh mouse, rat, dog and human blood using the indirect method (Yu *et al.*, 2005); compounds were incubated for 0.5 h at a concentration of 1 μM.

The PK of MRK-1, M1 and M2 in rat and dog were determined after single intravenous (0.5 mg/kg; 1.5 μmole/kg) and single oral (1.0 mg/kg; 3.1 μmole/kg) administration. Plasma from serial blood samples was analyzed quantitatively by LC-MS/MS. Plasma samples were prepared for analysis by means of a single step protein precipitation technique by adding 200 μL of IS crashing solvent (labetalol, alprazolam and diclofenac in acetonitrile) to 50 μL aliquots of plasma. Samples were mixed by vortex for homogeneity and then subjected to centrifugation for 10 minutes at 400 rpm. The supernatant (200 μL) was then transferred into new 96-well plates and injected into the LC-MS/MS for analysis. Chromatography was carried out by means of LX-2 Thermo Cohesive systems equipped with ThermoFisher Allegros Pumps (Thermo Fisher Scientific Inc., Cambridge, MA). Separation was performed on a Waters Acquity HSS T3 column (2.1 mm x 50 mm, 1.8 μm; Waters, Milford, MA) at room temperature with an injection volume of 5 μL. The mobile phase consisting of a solvent A (0.1% formic acid in water) and solvent B (0.1% formic acid in acetonitrile) was delivered at a flow rate of 750 μL/min. The LC gradient started from 95/5 (A/B) and changed to 5/95 (A/B) from 0.25 to 1.75 min (ramp) remaining constant to this ratio for 0.5 min. The gradient decreased to 95/5 (A/B) from 2.25 to 2.65 min (ramp) remaining constant to this ratio for 0.8 min. Detection was carried out using an API5000 triple quadrupole tandem mass spectrometer equipped with an electrospray interface (Applied Biosystems, Foster City, CA). Ions were created in the positive ion mode setting the sprayer voltage at 5.0 kV and the ion source temperature at 500°C. The common parameters and the nitrogen flow values for nebulizer gas (Gas 1), auxiliary gas (Gas 2), curtain gas and the gas for collision-activated dissociation (CAD) were set at 60, 60, 35 and 5, respectively. Detection of the analytes was performed in the multiple reaction-monitoring mode and the following precursor to product ion pairs were used for quantitation: m/z 325.3 → 221.2 for MRK-1 (DP/CE: 100/20); m/z 297.4 → 193.3 for M1 (DP/CE: 80/20) and m/z 339.1 → 235.2 for M2 (DP/CE: 100/25). The following MRM transitions were monitored for the IS: 329.2 → 162.1 for labetalol, 309.0 → 205.0

for alprazolam and 296.0 → 214.0 for diclofenac. Peak area ratios of the analyte to IS (labetalol) were utilized for construction of the calibration curve. A weighting of 1/x2 (least-squares linear regression analysis, where x is the concentration of a given standard) was used for curve fit. Concentrations in unknown samples were calculated from the best-fit equation ($y = mx+b$) where y is the peak area ratio. Non-compartmental analysis afforded estimates of plasma clearance (CL), volume of distribution at steady state (Vss), absorption rate constant (ka) and bioavailability (F). Fraction absorbed (fabs) was estimated from bioavailability and CL assuming CL to be exclusively hepatic with liver blood flows 84 mL/min/kg (rat) and 31 mL/min/kg (dog).

The CL of MRK-1, M1 and M2 in man were predicted by a range of techniques; single species allometry (Tang *et al.*, 2007), scaling of in vitro intrinsic clearance using physiological scaling factors and the well-stirred liver model (Ito and Houston, 2004), and hybrid allometry (Lavé *et al.*, 1999). The predicted human Vss was derived from the mean of the unbound Vss in rat and dog corrected for human plasma protein binding. The human ka of MRK-1 was assumed to be 1 /h and human fabs after oral administration of MRK-1 was assumed to be equivalent to that estimated from rat PK data.

Partial qualification of the model in the dog

The ability of the model to predict the observed PK in dog was assessed. The metabolite pathway flux approach was applied to the dog in an analogous manner to the human predictions. Estimated ka, fabs, CL and Vss were obtained from obtained from PK studies as described above. CL and Vss were used to derive elimination rate constants and these were then fractionated according to the relative pathway flux determined in dog hepatocytes. The dog data inputs used in the model are summarized in Table 1. The model was used to predict the plasma concentrations and AUCs of MRK-1, M1 and M2 following oral administration of MRK-1.

RESULTS

Metabolism of MRK-1, M1 and M2. Based on in vitro and in vivo studies, a putative metabolic pathway for MRK-1 was proposed (Figure 1). MRK-1 was found to be *N*-dealkylated to form M1 which then underwent *N*-acetylation to form M2. Metabolite M2 was also found to be formed directly from MRK-1 in microsomes and recombinant cytochromes P450. The ability of M2 to be formed both directly or via M1 was also indicated from in vitro studies with MRK-1 with a fully deuterated ethyl side chain (data not shown). The formation of M2 from M1 was also found to occur in rat blood during the assay to determine blood to plasma partitioning. This pathway was not observed in blood from dog or human. The conversion of M1 to M2 did not occur in dog hepatocytes. Quantitative data from human hepatocytes suggested that MRK-1 was metabolized predominantly to M1 and that M1 itself was metabolized mainly to inactive metabolites. The small amount of M2 formed either directly from MRK-1 or via M1 was predicted to be metabolized back to M1. The predicted fractional pathways in human are given in Table 1.

Partial qualification of the model in the dog. Unbound plasma AUCs of MRK-1, M1 and M2 in the dog following oral administration of MRK-1 were compared with the predictions from the model. The comparison of plasma profiles is shown in Figure 3. Predicted plasma concentrations of MRK-1 were similar to the observed values resulting in a predicted:observed AUC ratio of 1.01. For both M1 and M2, predicted plasma concentrations were lower than those observed with predicted:observed AUC ratios of 0.60 (M1) and 0.63 (M2).

Prediction of the human efficacious dose of MRK-1

Using the model inputs detailed in Table 1, including a target efficacious unbound AUC of 16.8 µM.h MRK-1 equivalents, the human efficacious dose of MRK-1 was predicted to be 2.7 mg/kg (8.2 µmole/kg) once daily; equivalent to approximately 187 mg (576 µmole for a 70 kg individual). The predicted relative contributions of MRK-1, M1 and M2 to the target efficacious

11

unbound exposure were 22%, 75% and 3% respectively and the predicted plasma profiles are

shown in Figure 4.

DISCUSSION

Active metabolites which contribute significantly to efficacy, likely result in increased complexity for drug development, including additional bioanalytical work to quantify metabolite(s) and increasingly complex PK/PD analyses. Indeed, it has been suggested that the formation of active metabolites must be avoided (Nassar *et* al., 2004) and their potential role in variable clinical response has been categorized as one reason for discontinuation of drug development under the heading of "inappropriate pharmacokinetics" (Smith *et al.*, 1996). Nonetheless, there are numerous examples of drugs where the pharmacology is either dominated by metabolites or where metabolites contribute significantly (Obach, 2013). There are also many cases of active metabolites being developed as drugs owing to superior pharmacological, PK or safety profiles compared to the parent molecule (Fura *et al.*, 2004). It has been proposed that interest in stable circulating metabolites from a purely toxicological standpoint will decline (Smith and Obach, 2010) since, at the time of their writing, there were few examples of linkage to toxicity outside of the pharmacology of the parent. Furthermore, it has been suggested that the risk of a metabolite being the sole perpetrator of a P450 inhibition-based DDI is low (Yu *et al.*, 2015). Nonetheless, regulatory guidelines exist for the characterization of human metabolites according to whether they are deemed to have been adequately tested during preclinical toxicology [Food and Drug Administration, 2012 (http://www.fda.gov/downloads/Drugs/GuidanceComplianceRegulatoryInformation/Guidances/UCM079266.pdf); International Conference on Harmonization, 2012 http://www.ich.org/products/guidelines/multidisciplinary/article/multidisciplinary-guidelines.html)]. Partially as a consequence of these guidelines, there has been much research into the prediction, detection and quantification of human circulating metabolites (Anderson *et al.*, 2009; Dalvie *et* al., 2009; Leclercq *et* al., 2009; Pelkonen *et al.*, 2009; Lutz *et al.,* 2010; Luffer-Atlas, 2012; Loi *et al.*, 2013). The theoretical basis for predicting metabolite exposure has been discussed by Lutz and coworkers (Lutz *et al.,* 2010). Perhaps driven by regulatory considerations, such efforts have largely been aimed at predicting the AUC ratio of metabolite:parent. The authors acknowledged

that some pharmacologic or toxicologic endpoints might be Cmax driven and that predictions of metabolite Cmax would require additional in vivo data on the metabolite. Recently, Nguyen and coworkers described a mechanistic approach for predicting the pharmacokinetics of midazolam and its metabolites using in vitro data and a physiologically based pharmacokinetic model (Nguyen *et al.*, 2016). The predicted AUC ratios of metabolite (1-OH and 4-OH midazolam) to parent were in good agreement with clinical observations and the model also afforded predicted plasma concentration versus time curves of midazolam and its metabolites. In the current study, since the metabolites were synthetically available, the model was parameterized so as to yield predictions of the full PK profile enabling risk *v.* benefit assessments to be made in the context of a life threatening disease and with metabolites likely contributing significantly to efficacy. The approach and model provided a pragmatic means to assess the feasibility of developing the parent molecule in terms of dose size and frequency as well as to evaluate follower molecules with similar potential for active metabolites. The model also facilitated the selection of toxicology species and dose levels towards establishing safety margins for the parent and its metabolites. The full executable model code is available (Supplemental Material 1) and may also be edited to explore other active metabolite scenarios, as described in Materials and Methods. However, in cases where the potency of the parent drug and active metabolite(s) diverge more than in the current work, or where simulations of different degrees of receptor occupancy or efficacy are required, it is advised to incorporate mutual competitive inhibition into the model (Ito *et al.*, 1993; Zhang *et al.*, 2009).

By visual inspection, the model provided a reasonable prediction of the observed PK of MRK-1, M1 and M2 in the dog (Figure 3) with AUC ratios (predicted:observed) of 1.01 (MRK-1), 0.60 (M1) and 0.63 (M2). Since MRK-1 was the compound administered, the model would have been expected to provide a good prediction of the observed data for MRK-1. However, inspection of Figure 3 suggests that concentrations at early timepoints are over predicted whilst at later timepoints they are under predicted. Inaccuracies in the non-compartmental parameter estimates (ka, CL, Vss) as well in the estimation of fabs, are likely to have contributed to these deviations.

For the metabolites M1 and M2, the formation rate intrinsic clearances in hepatocytes were usually derived from only the zero and first time point. It is possible that this contributed to the observed under prediction of M1 and M2 concentrations in dog and may also impact the human predictions; in future work of this type, a richer sampling protocol is indicated. A further potential source of error would be any clearance by non-hepatic metabolic mechanisms as this is not accounted for in the model. Analysis of urine and bile samples from studies in bile-duct cannulated rats and dogs (data not shown) suggested that MRK-1 was eliminated almost exclusively as metabolites. However, this does not rule out the potential for uptake-mediated clearance of MRK-1 and there is no data available on the in vivo clearance pathways for M1 and M2. The lack of conversion of M1 to M2 in dog hepatocytes was consistent with known *N*-acetylation species differences (Tibbits, 2003; Gao *et al.*, 2006; Loureiro *et al.*, 2013). Further qualification of the PK model using rat data would therefore clearly have been desirable; however the metabolism of M1 to M2 observed in rat blood, but not dog or human blood, rendered such a validation questionable both in terms of feasibility and value. Since the in vivo efficacy model was only available in the mouse, it was not possible to validate the dose prediction in another species. However, since such a model would employ human tumor cells lines in common with the mouse model, it would perhaps not be a true test of translatability. A further assumption of the model was that free plasma concentrations of MRK-1, M1 and M2 were a surrogate for the efficacious intratumoral concentrations. In vitro studies into the potential for active transport were inconclusive (data not shown) and no data were available on the expression of drug transporters in the tumor cell line. Therefore the relationship between plasma and tumor free drug levels is unknown but would be an area of focus for a more mechanistic understanding of the system. Despite these limitations, based on the partial qualification using dog data, and with the assumption that hepatic metabolism is the major clearance pathway for MRK-1, M1 and M2, the metabolic pathway fractionation approach and the model were deemed to be fit for purpose in a drug discovery setting.

For MRK-1, the predicted efficacious dose of 187 mg, once daily, was deemed to be feasible for further development with sufficient margin for error. As in the dog, the prediction accuracy may have been affected by issues such as inaccuracies in the estimation of formation rate intrinsic clearances and clearance by non-hepatic metabolic mechanisms. In addition, the model did not take into account the possibility of first pass extraction of MRK-1 by the gut and this is a potential area for future work to strengthen the model. The model predicted that the majority of the clinical efficacy would be driven by metabolite M1 and, as such, MRK-1 may be thought of as a prodrug even though it is active in its own right. M2 was predicted to contribute only 3% of the efficacious exposure equivalents, consistent with its relatively low fractional formation (0.02 from MRK-1 and 0.08 from M1; Table 1) and subsequent metabolism back to M1. The predicted elimination rate constants (Table 1) suggest that the half-life of M1 would be approximately 10 h in man, compared to 5.5 h for MRK-1, yielding a combined profile more suited to once daily administration than for MRK-1 without active metabolites. Conversion to the active metabolite M1 may therefore be deemed to be a very beneficial feature of MRK-1, both in terms of required dose size and administration frequency   In the model, either turning off the conversion of MRK-1 to M1, or making M1 pharmacologically inactive, both yielded a predicted human efficacious dose of approximately 800 mg MRK-1 daily, which is much less feasible from a formulation and development perspective. In this scenario, the predicted peak concentrations of MRK-1 are some four to five-fold higher, with the potential for a greater safety risk. To ameliorate these issues, it is likely that MRK-1, without its active metabolite, would be a b.i.d. drug.

In conclusion, the modeling approach described here facilitated a pragmatic prediction of the contribution of active metabolites to clinical efficacy for a discovery stage compound. The model afforded predictions of the clinically efficacious dose and was instrumental in the design of preclinical safety studies. Furthermore, the model was used to test "what if" scenarios and helped to guide further optimization of this chemical series within the discovery program.

ACKNOWLEDGEMENTS

AUTHORSHIP CONTRIBUTIONS

Participated in research design: Martin, Hill, Baker, Deshmukh, Mulrooney

Conducted experiments: Hill, Mulrooney

Contributed new reagents or analytic tools: Hill, Mulrooney

Performed data analysis: Martin, Hill, Mulrooney

Wrote or contributed to the writing of the manuscript: Martin, Hill, Baker, Deshmukh, Mulrooney

REFERENCES

Anderson S, Luffer-Atlas D, and Knadler MP (2009) Predicting circulating human metabolites: how good are we? *Chem Res Toxicol* **22:** 243-256.

Bauman JN, Frederick KS, Sawant A, Walsky RL, Cox LM, Obach RS, and Kalgutkar AS (2008) Comparison of the bioactivation potential of the antidepressant and hepatotoxin nefazodone with aripiprazole, a structural analog and marketed drug. *Drug Metab Dispos* **36:**1016-29.

Bueters T, Gibson CG, and Visser SA (2015) Optimization of human dose prediction by using quantitative and translational pharmacology in drug discovery. *Future Med Chem* **7**: 2351-69.

Dalvie D, Obach RS, Kang P, Prakash C, Loi CM, Hurst S, Nedderman A, Goulet L, Smith E, Bu HZ, and Smith DA (2009) Assessment of three human in vitro systems in the generation of major human excretory and circulating metabolites. *Chem Res Toxicol* **22:** 357-368.

Drayer DE (1976) Pharmacologically active drug metabolites: therapeutic and toxic activities, plasma and urine data in man, accumulation in renal failure. *Clin Pharmacokinet* **1:** 426-443.

Fura A (2006) Role of pharmacologically active metabolites in drug discovery and development. *Drug Discov Today* **11:**133-142.

Fura A, Shu YZ, Zhu M, Hanson RL, Roongta V, and Humphreys WG (2004) Discovering drugs through biological transformation: role of pharmacologically active metabolites in drug discovery. *J Med Chem* **47:** 4339-4351.

Gao W, Johnston JS, Miller DD, Dalton JT (2006) Interspecies differences in pharmacokinetics and metabolism of S-3-(4-acetylamino-phenoxy)-2-hydroxy-2-methyl-N-(4-nitro-3-

18

trifluoromethylphenyl)-propionamide: the role of N-acetyltransferase. *Drug Metab Dispos* **34**: 254-60.

.

Ho PC, Abbott FS, Zanger UM, and Chang TK (2003) Influence of CYP2C9 genotypes on the formation of a hepatotoxic metabolite of valproic acid in human liver microsomes. *Pharmacogenomics J* **3:** 335-42.

Isoherranen N, Hachad H, Yeung CK, and Levy RH (2009) Qualitative analysis of the role of metabolites in inhibitory drug-drug interactions: literature evaluation based on the metabolism and transport drug interaction database. *Chem Res Toxicol* **22:** 294-298.

Ito K, and Houston JB (2004) Comparison of the use of liver models for predicting drug clearance using in vitro kinetic data from hepatic microsomes and isolated hepatocytes. *Pharm Res* **21**: 785-792.

Ito K, Yamada Y, Nakamura K, Sawada Y, and Iga T (1993) Classification of benzodiazepine hypnotics in humans based on receptor occupancy theory. *J Pharmacokinet Biopharm* **21**: 31-41.

Lavé T, Coassolo P, and Reigner B (1999) Prediction of hepatic metabolic clearance based on interspecies allometric scaling techniques and in vitro-in vivo correlations. *Clin Pharmacokinet* **36**:211-231.

Leclercq L, Cuyckens F, Mannens GS, de Vries R, Timmerman P, and Evans DC (2009) Which human metabolites have we MIST? Retrospective analysis, practical aspects, and perspectives for metabolite identification and quantification in pharmaceutical development. *Chem Res Toxicol* **22**:280-93.

Loi CM, Smith DA, and Dalvie D (2013) Which metabolites circulate? *Drug Metab Dispos* **41**:933-51.

.

Lombardo F, Waters NJ, Argikar UA, Dennehy MK, Zhan J, Gunduz M, Harriman SP, Berellini G, Liric Rajlic I, and Obach RS (2013a) Comprehensive assessment of human pharmacokinetic prediction based on in vivo animal pharmacokinetic data, part 1: volume of distribution at steady state. *J Clin Pharmacol* **53**:167-177.

Lombardo F, Waters NJ, Argikar UA, Dennehy MK, Zhan J, Gunduz M, Harriman SP, Berellini G, Liric Rajlic I, and Obach RS. (2013b) Comprehensive assessment of human pharmacokinetic prediction based on in vivo animal pharmacokinetic data, part 2: clearance. *J Clin Pharmacol* **53**:178-91.

Loureiro AI, Fernandes-Lopes C, Bonifácio MJ, Wright LC, Soares-da-Silva (2013) *N*-acetylation of etamicastat, a reversible dopamine-β-hydroxylase inhibitor. *Drug Metab Dispos* **41**: 2081-2086.

Luffer-Atlas D (2012) The early estimation of circulating drug metabolites in humans. *Expert Opin Drug Metab Toxicol* **8:** 985-997.

Lutz JD, Fujioka Y, and Isoherranen N (2010) Rationalization and prediction of in vivo metabolite exposures: the role of metabolite kinetics, clearance predictions and in vitro parameters. *Expert Opin Drug Metab Toxicol* **6:**1095-1109.

Naritomi Y, Terashita S, Kagayama A and Sugiyama Y (2003) Utility of hepatocytes in predicting drug metabolism: comparison of hepatic intrinsic clearance in rats and humans in vivo and in vitro. *Drug Metab Dispos* **31:** 580-588.

Nassar AE, Kamel AM, and Clarimont C (2004) Improving the decision-making process in the structural modification of drug candidates: enhancing metabolic stability. *Drug Discov Today* **9:**1020-8.

Nguyen HQ, Kimoto E, Callegari E and Obach RS (2016) Mechanistic modeling to predict midazolam metabolite exposure from in vitro data. *Drug Metab Dispos* **44:** 781-791.

Obach RS (2013) Pharmacologically active drug metabolites: impact on drug discovery and pharmacotherapy. *Pharmacol Rev* **65:** 578-640.

Obach RS, Baxter JG, Liston TE, Silber BM, Jones BC, MacIntyre F, Rance DJ, and Wastall P (1997) The prediction of human pharmacokinetic parameters from preclinical and in vitro metabolism data. *J Pharmacol Exp Ther* **283**:46-58.

Pelkonen O, Tolonen A, Korjamo T, Turpeinen M, and Raunio H (2009) From known knowns to known unknowns: predicting in vivo drug metabolites. *Bioanalysis* **1:** 393-414.

Rambeck B, Sälke-Treumann A, May T, and Boenigk HE (1990) Valproic acid-induced carbamazepine-10,11-epoxide toxicity in children and adolescents. *Eur Neurol* **30:** 79-83.

Smith DA, Jones BC, and Walker DK (1996) Design of drugs involving the concepts and theories of drug metabolism and pharmacokinetics. *Med Res Rev* **16:** 243-266.

Smith DA, and Obach RS (2010) Metabolites: have we MIST out the importance of structure and physicochemistry? *Bioanalysis* **2:**1223-1233.

Tang H, Hussain A, Leal M, Mayersohn M, and Fluhler E (2007). Interspecies prediction of human drug clearance based on scaling data from one or two animal species. *Drug Metab Dispos* **35**: 1886-1893.

Tibbitts J (2003). Issues related to the use of canines in toxicologic pathology--issues with pharmacokinetics and metabolism. *Toxicol Pathol* **31** Suppl:17-24.

Yu H, Balani SK, Chen W, Cui D, He L, Humphreys WG, Mao J, Lai WG, Lee AJ, Lim HK, MacLauchlin C, Prakash C, Surapaneni S, Tse S, Upthagrove A, Walsky RL, Wen B, Zeng Z. (2015) Contribution of metabolites to p450 inhibition-based drug-drug interactions: scholarship from the drug metabolism leadership group of the innovation and quality consortium metabolite group. *Drug Metab Dispos* **43:** 620-630.

Yu S, Li S, Yang H, Lee F, Wu JT, Qian MG. (2005) A novel liquid chrmatograpy/tandem mass spectrometry based depletion method for measuring red blood cell partitioning of pharmaceutical compounds in drug discovery. *Rapid Commun. Mass Spectrom* **19**: 250-254.

Yu H and Tweedie D (2013) A perspective on the contribution of metabolites to drug-drug interaction potential: the need to consider both circulating levels and inhibition potency. *Drug Metab Dispos* **41:** 536-40.

Zhang X, Jones DR, and Hall SD (2009) Prediction of the effect of erythromycin, diltiazem, and their metabolites, alone and in combination, on CYP3A4 inhibition. *Drug Metab Dispos* **37**: 50-60.

.

Figure 1: Proposed metabolic pathway of MRK-1 derived from in vitro (hepatocytes), and in vivo (plasma from PK studies) data.

Figure 2: Schematic of the PK model constructed in Berkeley Madonna to predict the human pharmacokinetics of MRK-1, M1and M2.

Figure 3: Plasma concentrations of MRK-1, M1 and M2 observed following single oral administration of MRK-1 to dogs (1 mg/kg; 3.1 μmole/kg; mean of n=3) and predicted using the Berkeley Madonna PK model.

Figure 4: Predicted unbound plasma concentrations of MRK-1, M1 and M2 in human following once daily oral administration (187 mg to 70 kg individual = 2.7 mg/kg; 8.2 μmole/kg).

Table 1: Data Inputs, Designations in Model Script, and numerical values used for partial model qualification (dog) and prediction of MRK-1 efficacious dose (human). Asterisks indicate values calculated within the model; NA = not applicable to model qualification.

Data input	Molecule(s)	Designation in Model	Value (human)	Value (dog)
Fraction of MRK-1 parent eliminated to M1	MRK-1, M1	f_p_m1	0.93	0.44
Fraction of MRK-1 parent eliminated to M2	MRK-1, M2	f_p_m2	0.02	0.04
Fraction of MRK-1 parent eliminated to inactive metabolites*	MRK-1	f_p_xxx	0.05	0.52
Fraction of M1 eliminated to M2	M1, M2	f_m1_m2	0.08	0.00
Fraction of M1 eliminated to inactive metabolites*	M1	f_m1_xxx	0.92	1.00
Fraction of M2 eliminated to M1	M1, M2	f_m2_m1	0.73	1.00
Fraction of M2 eliminated to inactive metabolites	M2	f_m2_xxx	0.27	0.00
Absorption rate constant	MRK-1	Kap	1.0 /h	2.9 /h
Fraction absorbed	MRK-1	fabs	1.0	1.0
Plasma Clearance	MRK-1	CLp	4.8 mL/(min.kg)	10.1 mL/(min.kg)
Plasma Clearance	M1	CLm1	1.9 mL(min.kg)	1.6 mL/(min.kg)
Plasma Clearance	M2	CLm2	8.6 mL/(min.kg)	17.7 mL/(min.kg)
Volume of distribution	MRK-1	V1p	2.3 L/kg	1.0 L/kg
Volume of distribution	M1	V1m1	1.6 L/kg	1.1 L/kg
Volume of distribution	M2	V1m2	2.6 L/kg	2.1 L/kg
Elimination rate constant*	MRK-1	kep	0.125 /h	0.61 /h

Elimination rate constant*	M1	kem1	0.071 /h	0.087 /h
Elimination rate constant*	M2	kem2	0.198 /h	0.51 /h
Fraction unbound in plasma	MRK-1	fup	0.129	0.120
Fraction unbound in plasma	M1	fum1	0.238	0.238
Fraction unbound in plasma	M2	fum2	0.209	0.190
In vitro target binding potency	MRK-1	p_IC50	1.2 nM	NA
In vitro target binding potency	M1	m1_IC50	1.8 nM	NA
In vitro target binding potency	M2	m2_IC50	0.7 nM	NA
Molecular weight	MRK-1	mwp	324.38 Da	324.38 Da
Molecular weight	M1	mwm1	296.33 Da	296.33 Da
Molecular weight	M2	mwm2	338.36 Da	338.36 Da
Target unbound exposure for efficacy	MRK-1, M1, M2	TargAUCuUM410 equivs	16.8 µM.h	NA

MRK-1

Active metabolite M1
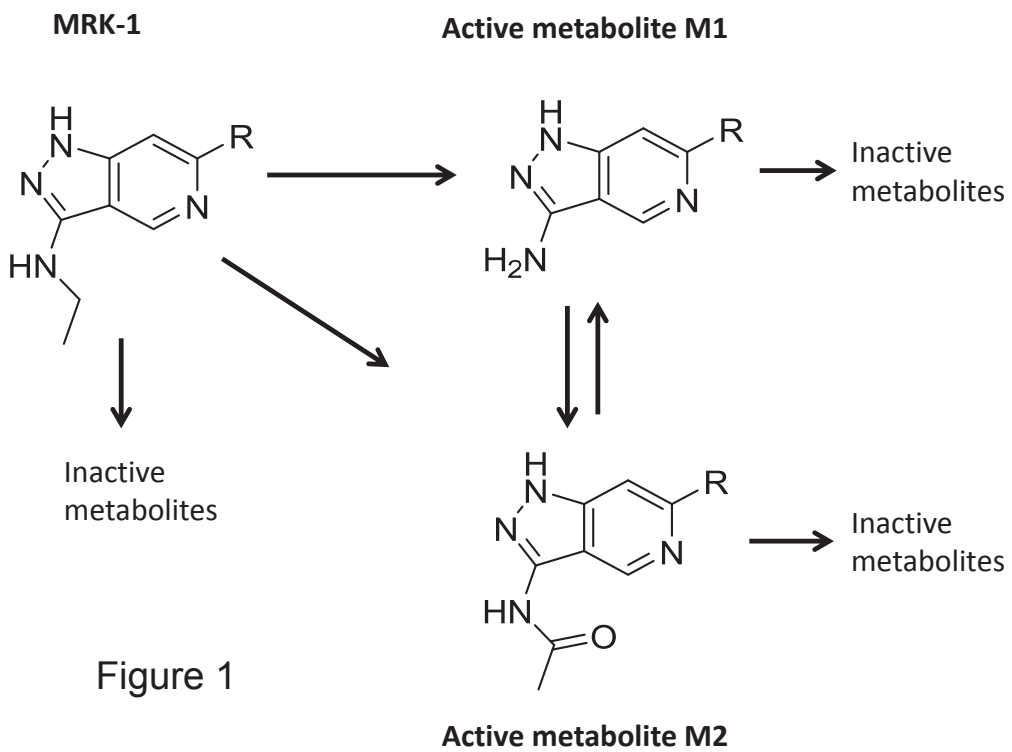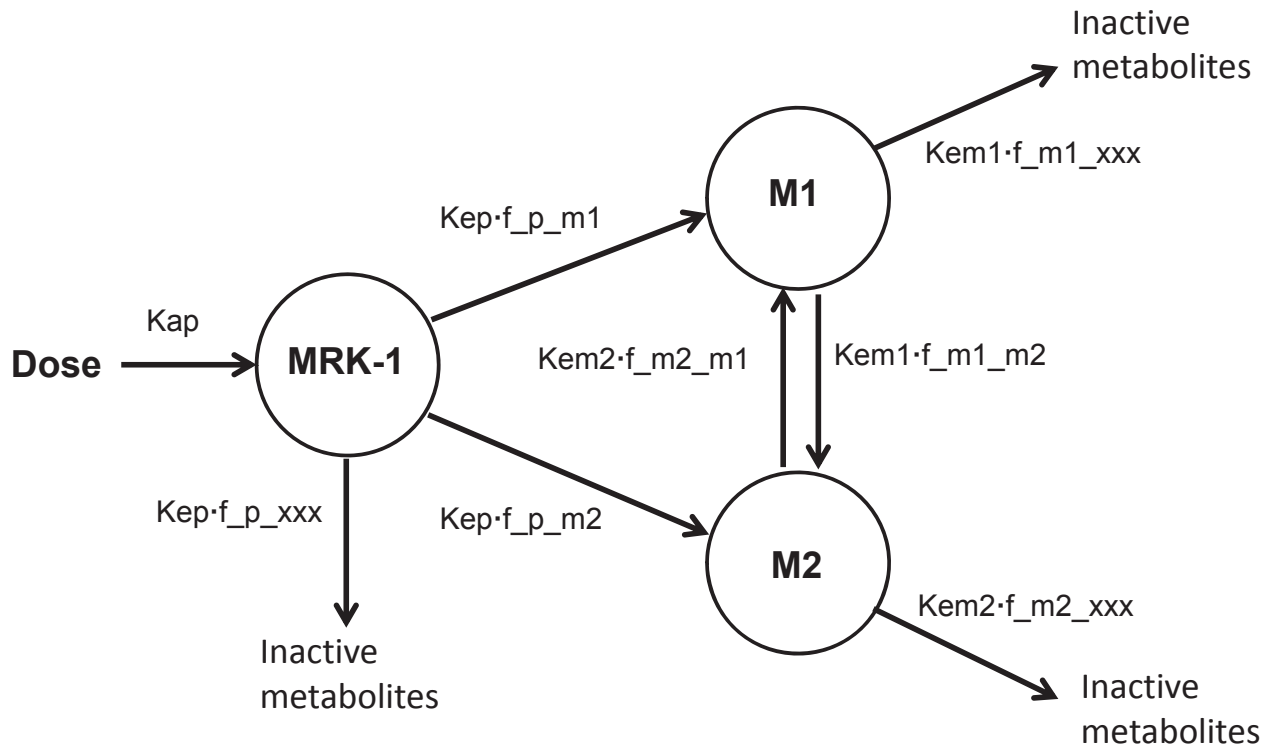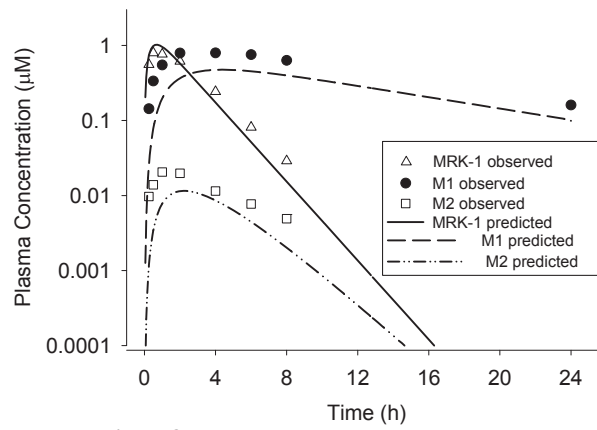
Inactive
metabolites

Inactive
metabolites

Inactive
metabolites

Figure 1

Active metabolite M2

Figure 2

Figure 3

Figure 4